ACS APPLIED MATERIALS & INTERFACES

Research Article

www.acsami.org

Controllable Synthesis of Highly Conductive Polyaniline Coated Silica Nanoparticles Using Self-Stabilized Dispersion Polymerization

Minkyu Kim, Sunghun Cho, Jooyoung Song, Suim Son, and Jyongsik Jang*

WCU program of Chemical Convergence for Energy and Environment (C2E2), School of Chemical and Biological Engineering, College of Engineering, Seoul National University, 599 Gwanak-ro, Gwanak-gu, Seoul 151-742, Korea

Supporting Information

ABSTRACT: Highly conductive silica/polyaniline (PANi) core/shell nanoparticles (NPs) were synthesized in various diameters (from 18 to 130 nm) using self-stabilized dispersion polymerization. The polymerization was carried out in an aqueous/organic liquid system at −30 °C. In this system, the organic phase plays a key role in directing para-direction oriented polymerization of the PANi on the surface of silica NPs. Because of its para-direction polymerized structure, the synthesized silica/PANi core/shell NPs exhibited enhanced electrical conductivity (25.6 S cm^{-1}) compared with NPs (1.4 S cm^{-1}) prepared by homogeneous polymerization. The conductivities and BET surface areas were 25.6 S cm^{-1}/170 m^2 g^{-1} (18 nm in diameter), 22.5 S cm^{-1}/111 m^2 g^{-1} (35 nm in diameter), 18.3 S cm^{-1}/78 m^2 g^{-1} (63 nm in diameter), and 16.4 S cm^{-1}/53 m^2 g^{-1} (130 nm in diameter). In this series, increased para-coupling along the polymer backbone was elucidated using several characterization techniques, including Fourier transform infrared (FTIR), X-ray diffraction (XRD), and nuclear magnetic resonance (NMR) spectroscopy. As-prepared silica/PANi core/shell NPs exhibited capacitance as high as 305 F g^{-1}.

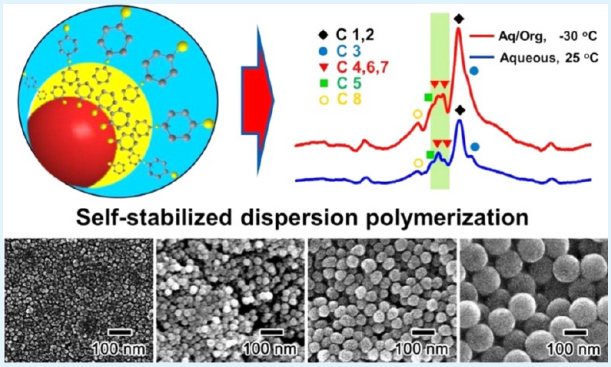

KEYWORDS: *polyaniline, silica, nanoparticles, conductivity, supercapacitors*

INTRODUCTION

The decreasing availability of energy from fossil fuels − coal, oil, and natural gas − and climate change are necessitating a societal shift toward the increased use of renewable and alternative energy resources. Developing low-cost, high-power, renewable, sustainable, safe energy sources for energy storage and energy production systems will be increasingly significant in the future.[1] As a result, much effort has been devoted to the fabrication of advanced devices for energy systems.[2−5]

Conducting polymers (CP) have attracted attention because of their potential to improve the electrode performance of energy storage devices.[6−8] Polyaniline (PANi) is the one of the most technologically promising CPs because of its unique redox behavior, low cost, environmental and chemical stability, and relatively high conductivity.[9−11] PANi having a small particle size and high conductivity can provide an increased electroactive area[12−14] and fast electron transmission during redox reactions,[15−17] both of which boost high capacitance performance.[18] Thus, highly conductive PANi nanostructures are promising materials for batteries and supercapacitors.[19−21] Although several structures have been reported to increase the surface area to volume ratio of PANi, such as micrometer or nanometer-sized PANi-coated polymeric latex particles[22] or silica spheres,[23,24] the synthesis of nanosized and highly conductive PANi is still challenging.

Inorganic/polymer core/shell nanocomposites have been extensively studied, and the synthesis of nanoscale polymers without aggregation of nanoparticles (NPs) has been a particular focus of many of these efforts. Additionally, the use of a silica core presents some advantages like high colloidal stability and easily controllable particle size. However, previously reported micro/nanosized silica/CP core/shells typically exhibit relatively low conductivity,[22,24] which is a crucial limiting factor for high-performance supercapacitors. Therefore, fabrication of a coating of inorganic NPs as CPs with high electrical conductivity and large surface area is still needed and challenging.

In this study, we developed a new synthetic method for the fabrication of silica/PANi core/shell NPs having high electrical conductivity using self-stabilized dispersion polymerization[25] (SSDP) and an aqueous/organic liquid system at a low temperature of −30 °C. In our previous research, we synthesized silica/PANi core/shell NPs that exhibited electrical conductivity of 1.4 S cm^{-1} in a homogeneous system.[24] The polymerization of PANi proceeded principally in the para-direction, and the synthesized core/shell NPs exhibited enhanced electrical conductivity (25.6 S cm^{-1}). The polymeric

Received: June 1, 2012
Accepted: August 27, 2012
Published: August 27, 2012

   dx.doi.org/10.1021/am300979s | ACS Appl. Mater. Interfaces 2012, 4, 4603−4609

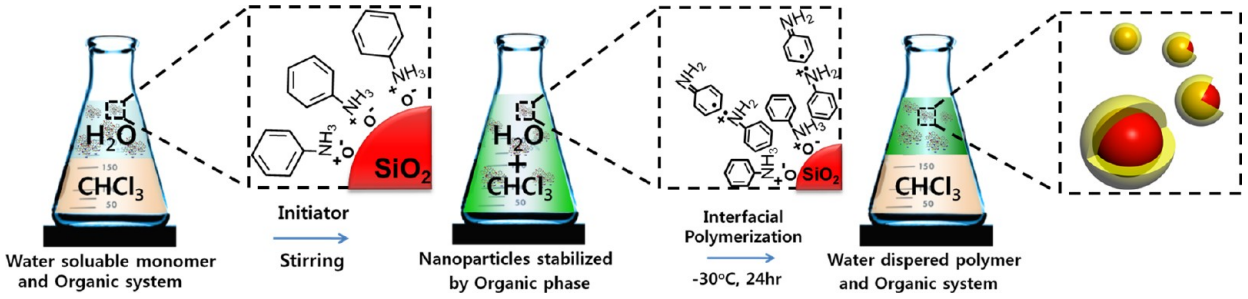

Figure 1. Illustrations of the sequential steps for synthesis of the silica/PANi core/shell.

backbone structure of the PANi on the silica surface was systematically investigated to elucidate the origin of the high electrical conductivity. Additionally, the obtained silica/PANi core/shell NPs exhibited improved electrochemical properties compared to NPs prepared by homogeneous polymerization when evaluated as the electrode materials for supercapacitors.

EXPERIMENTAL SECTION

Materials. Aniline (C_6H_7N, ≥99.5%), ammonium persulfate ($[NH_4]_2S_2O_8$, 98%), hydrochloric acid (HCl, 37%), ammonia solution (28−30%), and chloroform ($CHCl_3$, ≥99.8%) were purchased from Aldrich Chemical Co. Deionized water was used as a chemical solvent for aniline. Silica NPs (diameter: 12 and 22 nm) were purchased from Aldrich Chemical Co. The 50 and 100 nm silica NPs were synthesized using tetraethyl ortho silicate and ammonia solution.

Synthesis of Silica/PANi Core/Shell NPs (SP1). At first, the silica NPs (3.8 mmol) was added to deionized water (40 mL). An anilinium solution, aniline (2.1 mmol) and HCl (8.2 mmol) added to deionized water (11 mL), was injected to the above-prepared solution under vigorous stirring condition (with magnetic stirring bar) and the reaction proceeded for 1 h at 0 °C. Then, the mixed solution was injected to the chloroform (80 mL) in Erlenmeyer flask with mechanical stirrer at −30 °C. Subsequently, ammonium persulfate (APS) solution (0.854 M, 2 mL) was injected to the mixture as initiator in a dropwise fashion. The reaction was performed until the color of the solution changed from opaque to dark green, which represents the metallic states of chemically doped PANi:emeraldine salt (ES). After the polymerization, the silica/PANi core/shell NPs were precipitated by centrifugal precipitation and washed with distilled water, ethanol, and acetone to remove residual agents. The size of the silica/PANi core/shell NPs were controlled by varying the size of silica cores (from 12 to 100 nm). In each procedure, other reaction conditions are identical to those described above.

Homogeneous Synthetic Method for SP2 and Bulk PANi. The silica NPs (3.8 mmol) was added to distilled water (40 mL). An anilinium solution, aniline (2.1 mmol) and HCl (8.2 mmol) were dissolved in deionized water (11 mL), was added as dropwise to the above-prepared solution, and stirred for 1 h under vigorous stirring. An APS solution (0.854 M, 2 mL) was added to the aniline/silica solution. The polymerization of aniline was carried out at room temperature (25 °C) for 12 h. After the polymerization, a dispersion solution of the silica/PANi core/shell NPs was obtained by centrifugation and redispersion of the NPs in distilled water, ethanol, and acetone. The size of the silica/PANi core/shell NPs were controlled by varying the size of silica cores (from 12 to 100 nm). In each procedure, other reaction conditions are identical to those described above.

In the case of bulk PANi, aniline (0.01 M) was dissolved in HCl (0.9 M, 35 mL) solution at room temperature (25 °C) by magnetic stirring for 15 min. An APS solution (0.5 M, 10 mL) was added to the solution which was magnetically stirred for 15 min and then stirring was kept for 6 h. The polymerization was stopped when the color of the solution changed to dark-green, which represents the ES states of chemically doped PANi. The prepared PANi was precipitated by centrifugal precipitation and washed with distilled water, ethanol, and acetone to remove residual agents. Finally, the green colored PANi nanofibers were obtained.

Electrochemical Measurements. The electrode for the supercapacitor was prepared as follows. The 2.2 mg of silica/PANi core/shell NPs was mixed with polymeric binder (Polytetrafluoroethylene, 0.22 mg) and carbon black (0.22 mg). The mixture was coated on a stainless steel mesh (1 × 1 cm^2) which is known to be stable in acidic condition. The coated mixture was rolled by a bar-coater to form a sheet type. Subsequently, the molded electrode as dried at 25 °C for 12 h before use. Cyclic voltammetric measurements were performed in the standard three-electrode system; Ag/AgCl is used as the reference electrode, and a platinum wire (6 cm) is used as the counter electrode in 1 M H_2SO_4 solution as electrolyte at a sweep rate of 30 mV s^{-1}. The galvanostatic charge/discharge tests at the current densities of 2.6 A g^{-1} were performed by cycling potential from 0 to 0.8 V in 1 M H_2SO_4.

Characterization. Photographs of transmission electron microscope (TEM) were obtained with a LIBRA 120 (Carl Zeiss, Germany). In the sample preparation, nanomaterials diluted in ethanol were cast onto a copper grid. A JEOL 6700 (JEOL, Japan) was used to obtain field-emission scanning electron microscope (FE-SEM) images and energy dispersive X-ray spectroscopy (EDX) graphs. The X-ray diffraction (XRD) was recorded on a New D8 Advance (Bruker, Germany). The fouriertransform infrared (FTIR) spectrum was recorded on a MB 100 spectroscope (Bomem, Canada) in the absorption mode. Avance II (Bruker, Germany) was used to obtain solid-state ^{13}C NMR spectra. The measurement of the electrical conductivity was carried out with a KEITHLY 2400 by a four-probe method (KEITHLY, USA). Nitrogen adsorption/desorption isotherms were measured using Micromeritics ASAP 2000 at 77 K. The electrochemical measurements were performed with a Wonatech WBCS3000 potentiostat, which was measured in a conventional three-electrode beaker type cell in 1 M H_2SO_4 solution as electrolyte at 25 °C.

RESULTS AND DISCUSSION

Silica/PANi NPs (SP1) were synthesized by SSDP, as illustrated in Figure 1. First, silica NPs were dispersed in aqueous solution to serve as templates for adsorption of aniline monomers. Then, anilinium hydrochloride monomer ions were added to the silica NP solution. The monomer ions preferentially located on the surface of the silica NPs due to charge−charge interactions between the positively charged amine of the monomer and the negatively charged silica surface. After stirring for 1 h, chloroform was added to the monomer-impregnated silica NP solution to lower the melting temperature of the solution. When the temperature of the reaction solution dropped to −9 °C, the solubility of the anilinium hydrochloride in the aqueous phase decreased and became distributed in both the aqueous and organic (chloroform) phases.[25] Thus, through the $\pi-\pi$ stacking, additional anilinium hydrochloride monomer was adsorbed onto the surface of silica where monomer ions were prelocated.[26,27] After injection of

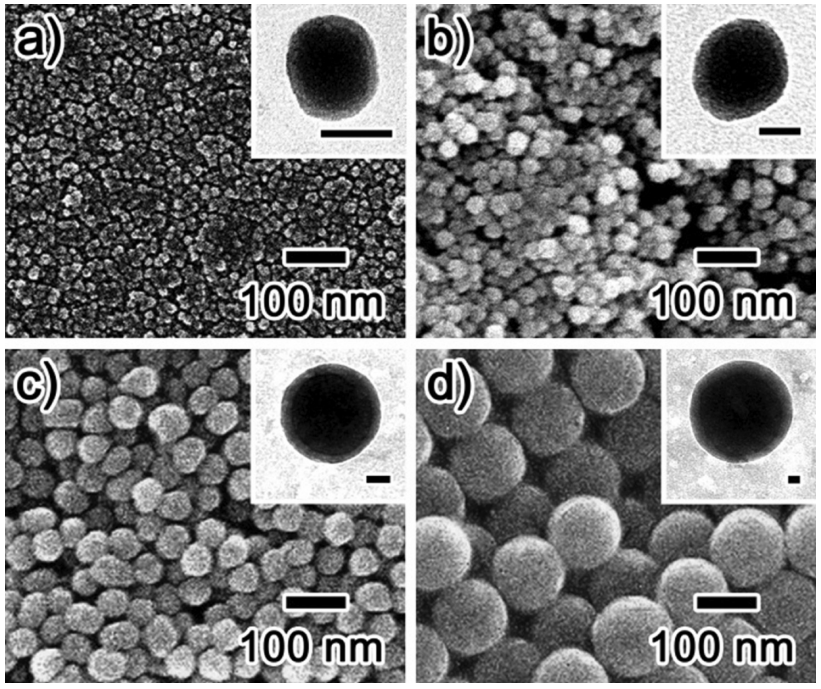

Figure 2. FE-SEM images and TEM images (inset) of SP1with the average size of (a) 18, (b) 35, (c) 63, and (d) 130 nm. The scale bars of inset images represent 15 nm.

APS as a water-soluble initiator, polymerization of monomer was initiated near the surface of the silica NPs. The growing PANi chains moved toward the interface between the aqueous and organic phases as result of insolubility in both aqueous and organic phases.[24,28,29] With both a hydrophilic part (amine group) and a hydrophobic part (phenyl ring), anilinium hydrochloride monomers acted as surfactant.[25,30,31] Because the monomers and growing polymer chains acted as interfacial stabilizers, the organic phase could be well dispersed in the aqueous reaction medium. Additionally, the organic phase tended to separate the aniline monomers and grown PANi chains from the reactive ends of the chains in the aqueous phase. As a result, undesirable side reactions, such as ortho-coupling or Michael reductive additions, were suppressed, and the polymerization proceeded mainly in the para-direction (see Figure S1 in the Supporting Information).[25,28,29] After 24 h of polymerization at −30 °C, green SP1 was obtained.

Figure 2 shows field-emission scanning electron microscopy (FE-SEM) and transmission electron microscopy (TEM) images of SP1 particles of various diameters (*ca.* 18, 35, 63, and 130 nm). The size of the SP1 could be controlled by varying the size of silica core NPs. The histograms of the particle size distributions are shown in Figure S2 in the Supporting Information. The core/shell structure of SP1 was confirmed by TEM observation. The insets in Figure 2 clearly show that the silica NPs were encapsulated by a thin polymer shell. These results indicate that silica NPs of various sizes were successfully coated with polymer shell *via* SSDP. Based on the microscopic images, it could be considered that the SP1 has the similar shape as the previously synthesized core/shell NPs (SP2).[24] The compositions of pristine silica NPs and SP1 were also investigated by energy-dispersive X-ray spectroscopy (EDX) (Table 1). Compared to the pristine silica NPs, the %C values of the SP1 increased, whereas the %O and %Si values decreased because of existence of PANi on the silica surface. Notably, the detection of nitrogen, attributable to amine groups in PANi, confirms the existence of PANi on the surface of the silica NPs. In addition, the observation of chloride atoms in the SP1 indicates the hydrochloric acid doping state of the PANi. The detection of carbon in the pristine silica sample could be attributed to the carbon tape used for fixing the samples onto the EDX specimen mount. From these data, it was concluded that SP1 was successfully synthesized via the SSDP method, and the diameter of the NPs could be controlled by varying the size of the silica core.

Table 1. Weight Ratio of the Pristine Silica and Silica/PANi Core/Shell NPs Measured by EDX

element percentage (wt %)	pristine silica NPs	silica/PANi core/shell NPs
C	7.99	37.47
O	64.69	35.98
Si	27.33	16.55
N	0.00	7.31
Cl	0.00	2.69
totals	100	100

Fourier-transform infrared (FTIR) spectroscopy of SP1 was also used to confirm the SSDP polymerization of PANi (Figure 3a). Silica/PANi core/shell NPs prepared by homogeneous dispersion polymerization (SP2) were used for comparison. In the spectra of both SP1 and SP2, characteristic PANi peaks were observed at 1582, 1484, and 1310 cm^{-1}, originating from quinone ring deformation, phenyl ring deformation, and C−N stretching of a secondary aromatic amine, respectively.[28,29] The existence of these peaks demonstrated the successful polymerization of PANi on the surface of the silica NPs.

X-ray diffraction (XRD) and nuclear magnetic resonance (NMR) analyses were performed to investigate the para-direction polymerization. XRD patterns of the core/shell NPs in the emeraldine base (EB) state are shown in Figure 3b. EB-state PANi was obtained by deprotonation of the emeraldine salt (ES) state of PANi in the SP1 with 0.8 M ammonia

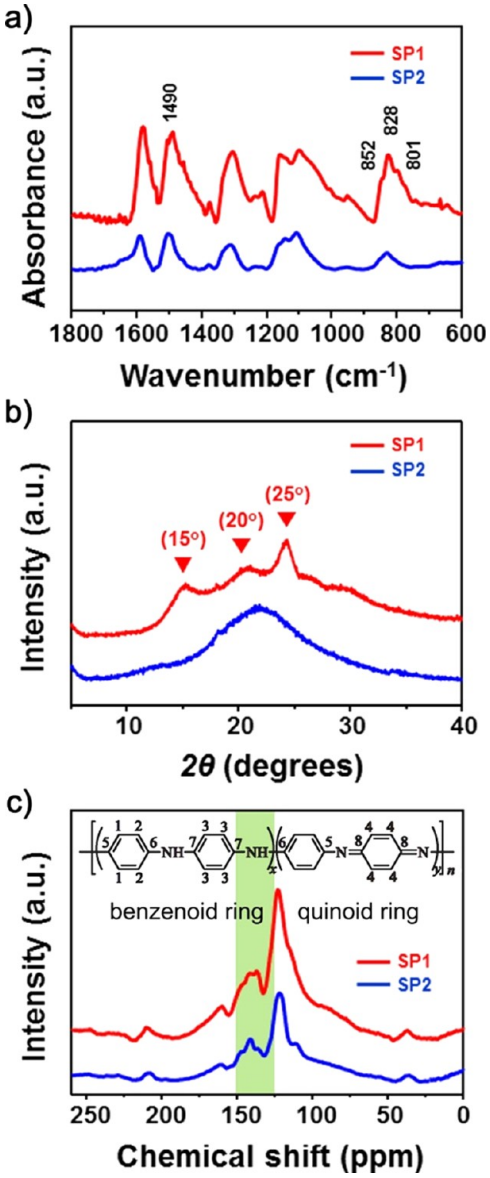

Figure 3. (a) FTIR spectra of the silica/PANi core/shell NPs prepared by self-stabilized polymerization method (SP1, red line) and homogeneous dispersion polymerization method (SP2, blue line); (b) X-ray diffraction patterns and (c) solid-state ^{13}C NMR spectra of the EB state SP1 (red line) and SP2 (blue line).

solution. The SP2, which was prepared *via* homogeneous dispersion polymerization, exhibited a broad scattering background in its spectra, indicating that the amorphous region dominated the PANi of SP2.[30,31] On the other hand, background peaks in the spectra of SP1 obviously decreased, and intense peaks at 15, 20, and 25° appeared. The *d*-spacing (~3.5 Å) associated with the diffraction peak at 25° corresponds to the face-to-face interchain stacking distance between phenyl rings.[30,31] Thus, the increased peak intensity at 25°, along with the decrease in background intensity, implies improved $\pi-\pi$ interchain stacking. These results suggest a more planar chain conformation with reduced torsion angles between the phenyl rings and the plane of the backbone, resulting in elongation of the effective conjugation length. Additionally, the increase crystallinity of SP1 also induces the improvement of conductivity. It is well-known that conducting polymers with higher conductivities are obtained in more homogeneous systems with a high degree of crystallinity.[39−42] In the conductivity model of CPs, electrons are transported along electronically isolated ordered regions through disordered regions where the electrons readily become localized. Consequently, the delocalization length of the electrons relies on the length of the ordered region between the disordered regions. Based on previous studies[32−42] and XRD analysis, it is believed that the highly conductive and crystalline PANi was successfully fabricated on the SiO_2.

Figure 3c shows the ^{13}C cross-polarization and magic-angle spinning nuclear magnetic resonance (^{13}C CP−MAS NMR) spectra of the SP1 in the EB state. The combined ^{13}C CP−MAS NMR technique is very powerful for resolving different microstructures present in the PANi shell. Four characteristic peaks were observed at 123, 137, 141, 148 (shoulder), and 158 ppm relative to tetramethylsilane. The clear peaks could be attributed to the ideal structure of PANi, as shown in the inset of Figure 4c: a peak at 158 (nonprotonated carbon 8), a

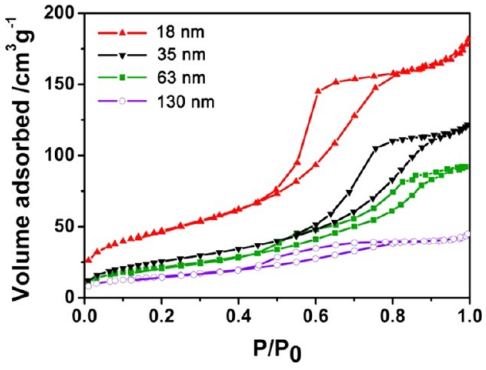

Figure 4. Nitrogen adsorption/desorption isotherms of different sized silica/PANi NPs: 18 nm (red line), 35 nm (green line), 63 nm (black line), and 130 nm (purple line).

shoulder at 148 ppm (nonprotonated carbon 5), peaks around 140 ppm (carbons 6, 7 and quinoid carbon 4), peak at 123 ppm (benzenoid carbons 1, 2), and a shoulder at 113 ppm (benzenoid carbon 3).[25] It is important to note that the SP1 presented two distinct peaks around 137 ppm in its spectra, while the SP2 exhibited only one peak in this region. These two peaks in SP1 correspond to the idealized repeat structure of the EB-state PANi. The protonated carbons (C4) in the quinoid ring, without rotation around the bent linkage of the imine group (=N−), contributed two structures that appeared as two peaks around 137 ppm.[43,44] In other words, the SP1 has an idealized EB repeat structure in its polymeric backbone, mainly oriented in the para-direction. These results indicate that the PANi shell synthesized according to the SSDP method in this study had much greater para-direction-oriented aniline in its polymeric backbone compared to the PANi shell prepared by homogeneous dispersion polymerization.

Nitrogen sorption experiments were performed to characterize the textural properties of different sized silica/PANi core/shell NPs. The nitrogen adsorption−desorption isotherms are displayed in Figure 4. The BET surface areas were ca. 170, 111, 78, and 53 $m^2\ g^{-1}$ for diameters of 18, 35, 63, and 130 nm, respectively; thus, surface area was inversely proportional to the size of the silica NPs.

To investigate the electrical conductivity of the silica/PANi NPs, the material was pressed and prepared into disk-shape samples. The conductivity of bulk PANi (see Figure S3 in the

Supporting Information) prepared via homogeneous dispersion polymerization was also measured similarly for comparison. The electrical conductivities of the samples were measured by the four-probe method (Table 2). The electrical conductivity of

Table 2. Electrical Conductivities of the Silica/PANi Core/Shell NPs

	conductivity (S cm^{-1})			
samples	18 nm	35 nm	63 nm	130 nm
SP1[a]	25.6	22.5	18.3	16.4
SP2[b]	1.42	0.74	0.58	0.32

[a]The self-stabilized dispersion polymerization was applied for the fabrication of SP1 samples. [b]The SP2 samples were synthesized by homogeneous dispersion polymerization.

the bulk PANi was found to be about 0.5 S cm^{-1}. The conductivities of core/shell NPs with diameters of 18, 35, 63, and 130 nm were measured to be ca. 25.6, 22.5, 18.3, and 16.4 S cm^{-1}, respectively. On the other hand, the electrical conductivities of the SP2 were found to be ca. 1.42, 0.74, 0.58, and 0.32 S cm^{-1} for samples with diameters of 18, 35, 63, and 130 nm, respectively. An improvement in the electrical conductivity of the SP1 samples (1 order of magnitude higher than for the SP2 and bulk PANi) was achieved by increasing the purity of the materials and by aligning the polymer chains. The electrical conductivity of CPs is strongly affected by the molecular structure and the polymer chain alignment.[30,31] Intramolecular electron transport is restricted by structural defects or impurities in conjugated structures, because CPs are principally one-dimensional systems with a typical conjugated backbone structure.[30,31] Therefore, the enhanced electrical conductivity of the SP1 originated from reduced structural defects in the polymer backbone and the para-direction-oriented polymerization. In addition, the electrical conductivities increased as the size of conducting NPs decreased in both SP1 and SP2 (from ca. 0.32 to ca. 1.42 S cm^{-1} in SP1 and from ca. 16.4 to ca. 25.6 S cm^{-1} in SP2). The smaller particles exhibited higher compactness and order when they were pressed into disks, thus leading to higher conductivity.[45]

The synthesized nanomaterials were prepared as electrodes for cyclic voltammetry (CV) tests, and galvanostatic charge/discharge was employed to evaluate the electrochemical properties and the capacitance performances. The specific capacitance of the electrodes could be calculated according to the following equation from CV curves

$$C = \int \frac{IdV}{vmV} \quad (1)$$

where C is the specific capacitance based on the mass of electroactive materials (F g^{-1}), I is the response current (mA), V is the potential (V), v is the potential scan rate (V s^{-1}), and m is the mass of the active electrode materials (mg).

Figure 5a shows the CV curves of SP1 (18, 35, 63, 130 nm) and SP2 (18 nm) at a scan rate of 30 mV s^{-1} in 1 M H_2SO_4 solution. In the case of the SP1, there are two pairs of redox peaks, indicating the pseudocapacitive characteristic of PANi. The first redox peak originated from the redox transition of PANi from a semiconducting state (leucoemeraldine state) to a conducting ES state. Faradaic transformation from emeraldine to pernigraniline is ascribed to the second redox peak.[46] However, the SP2 (18 nm) exhibited a CV curve without obvious redox peaks, because the SP2 (18 nm) had relatively

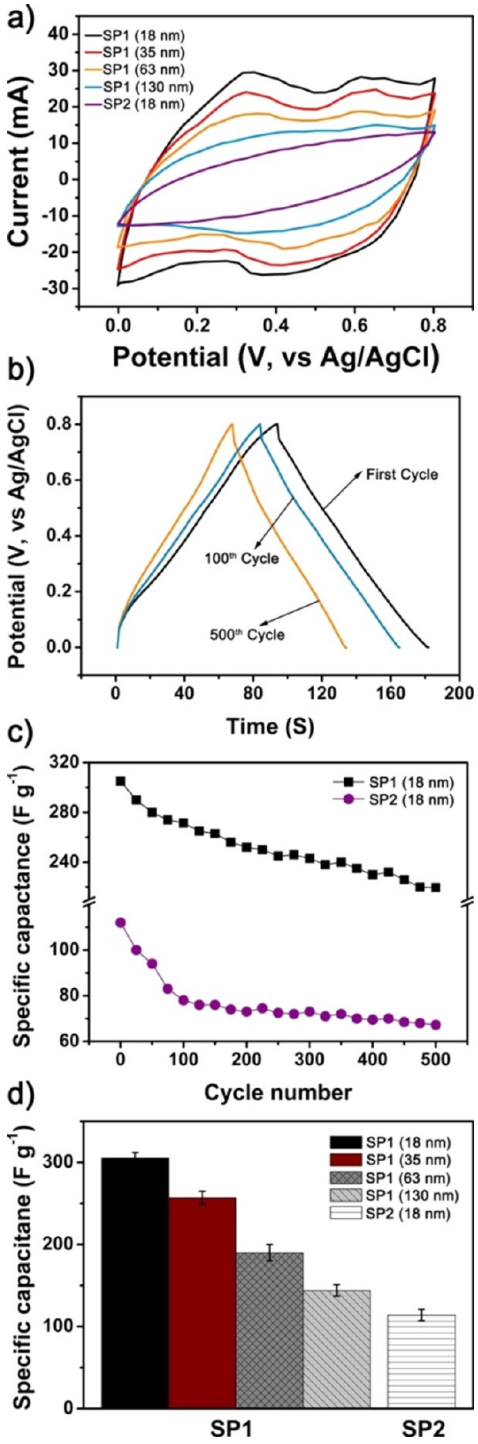

Figure 5. (a) Cyclic voltammograms of SP1 (18, 35, 63, 130 nm) and SP2 (18 nm) at 30 mV s^{-1} between 0 and 0.8 V in 1 M H_2SO_4 solution; (b) galvanostatic charge/discharge curve of SP1 (18 nm) at current density of 2.6 A g^{-1} in 1 M H_2SO_4 solution; (c) specific capacitances of SP1 (18 nm) and SP2 (18 nm) as a function of cycle number at a current density of 2.6 A g^{-1} in 1 M H_2SO_4 solution; (d) specific capacitances of SP1 (18, 35, 63, 130 nm) and SP2 (18 nm) at 30 mV s^{-1} between 0 and 0.8 V in 1 M H_2SO_4 solution.

low conductivity, which reduced the conducting network available for facile redox reaction of PANi.[47] The CV curves for SP1 samples exhibited large rectangular areas and high current response, suggesting that SP1 supercapacitors could be made to have large capacitance.[48] Specific capacitance values of

dx.doi.org/10.1021/am300979s | ACS Appl. Mater. Interfaces 2012, 4, 4603−4609

SP1 samples, calculated using eq 1, were found to be 305, 257, 190, and 144 F g^{-1} for materials with diameters of 18, 35, 63, and 130 nm, respectively. The smaller (more conductive) SP1 exhibited higher specific capacitance. The high capacitance and capacitance tendency of SP1 samples were attributed to the following two factors: first, the smaller size of SP1 provided larger electrode/electrolyte interface areas, which could provide electrochemical accessibility to the electrolyte through the interface of PANi.[46] Thus, SP1 with large surface area could present the high capacitance performance by effective access of electrolyte to electrode in the redox mechanism.[14] second, the more highly conductive PANi offered a higher conductivity path, facilitated a rapid charge/discharge process, and improved the redox activity.[49] The highly conductive path in SP1 originated from the enhanced conducting network that facilitated electron transfer in the electrode during the charge/discharge process.[49] The PANi network in SP1 is helpful for increasing electron transfer and the transport rate of electrolyte ions in the diffusion layer, both of which enhance the capacitance of the SP1 electrode.[47] Compared to SP1, the CV curve for SP2 (18 nm) exhibited small rectangular areas and a specific capacitance of 112 F g^{-1}. The SP1 (18 nm, 305 F g^{-1}) exhibited enhanced specific capacitance compared with SP2 (18 nm, 112 F g^{-1}). The SP1 (18 nm) presents high specific capacitance (305 F g^{-1}) compared to not only SP2 (18 nm, 112 F g^{-1}) but also previously reported nanostructured-PANi.[48−54] The specific capacitance of each nanocomposite studied by CV is summarized in Figure 5d.

The electrochemical stability of the SP1 (18 nm) was also investigated using cycled galvanostatic charge/discharge methods (Figure 5b). On the basis of the charge/discharge time, the charge storage capacity loss of SP1 was calculated as 12% loss after 100 cycles and 28% loss after 500 cycles. As shown in Figure 5c, the charge storage capacity of the SP2 (18 nm) decreased more rapidly (30% loss after 100 cycles and 40% loss after 500 cycles) compared with that of the SP1 (18 nm). At the cycle-life test, the dope or dedope of H^+ into or from the PANI chains on the SiO_2 results in the mechanical degradation like a swelling, breaking, and shrinkage of the nanostructured PANi, thus, leading to fading of capacitance.[13,55−57] In comparison to the SP2 electrode, the better cycle life of SP1 maybe mainly caused by increase crystalline region at backbone of PANi, which provide higher density to PANi and improved resistance toward change of the nanostructure of PANi at the cycle-life test.[58]

In conclusion, we successfully coated highly conductive and crystalline PANi onto silica NPs using the SSDP method. The diameter of the NPs was controlled from 18 to 130 nm by varying the size of the silica core. As the diameter of the silica/PANi core/shell NPs decreased (from 130 to 18 nm), the electrical conductivity increased (from 16.4 to 25.6 S cm^{-1}). When applied as potential electrode materials for supercapacitors, the synthesized silica/PANi core/shell NPs exhibited capacity as high as 305 F g^{-1} and had enhanced cycle-life performance compared to NPs prepared by homogeneous polymerization. The high conductivity and large surface area facilitated the charge/discharge of PANi, and the increased crystalline structure of PANi prevented severe deterioration of the polymer structure. The highly conductive and crystalline silica/PANi NPs prepared by SSDP can be used in various applications, such as batteries, sensors, actuators, corrosion protection, electro-optics, electro-chromic devices, and dye-sensitized solar cells.

■ ASSOCIATED CONTENT

Ⓢ Supporting Information

The schematic diagram of self-stabilized polymerization mechanism of the SP1 in aqueous/organic phase (Figure S1), size distribution histograms of the SP1 with different diameters (Figure S2), and TEM image of the bulk PANi (Figure S3). This material is available free of charge via the Internet at http://pubs.acs.org/.

■ AUTHOR INFORMATION

Corresponding Author

*E-mail: jsjang@plaza.snu.ac.kr. Tel: (+82) 2-880-7069. Fax: (+82) 2-888-1604.

Notes

The authors declare no competing financial interest.

■ ACKNOWLEDGMENTS

This research was supported by WCU (World Class University) program through the National Research Foundation of Korea funded by the Ministry of Education, Science and Technology (R31-10013).

■ REFERENCES

(1) Simon, P.; Gogotsi, Y. *Nat. Mater.* **2008**, *7*, 845−854.
(2) Wu, G.; More, K. L.; Johnston, C. M.; Zelenay, P. *Science* **2011**, *332*, 443−447.
(3) Armand, M.; Tarascon, J. M. *Nature* **2008**, *451*, 652−657.
(4) Lee, C. T. *J. Ind. Eng. Chem.* **2012**, *18*, 218−222.
(5) Lee, S. G.; Park, K. H.; Shim, W. G.; Balathanigaimani., M. S.; Moon, H. *J. Ind. Eng. Chem.* **2011**, *17*, 450−454.
(6) Huang, J. Y.; Wang, K.; Wei, Z. X. *J. Mater. Chem.* **2010**, *20*, 1117−1121.
(7) Zhao, G. Y.; Li, H. L. *Microporous Mesoporous Mater.* **2008**, *110*, 590−594.
(8) Wang, K.; Huang, J. Y.; Wei, Z. X. *J. Phys. Chem. C* **2010**, *114*, 8062−8067.
(9) Wang, Y.; Wang, X.; Li, J.; Mo, Z.; Zhao, X.; Jing, X.; Wang, F. *Adv. Mater.* **2001**, *13* (20), 1582−1585.
(10) Liu, W.; Kumar, J.; Tripathy, S.; Senecal, K. J.; Samuelson, L. *J. Am. Chem. Soc.* **1999**, *121*, 71−78.
(11) Gustafsson, G.; Cao, Y.; Treacy, G. M.; Klavetter, F.; Colaneri, N.; Heeger, A. J. *Nature* **1992**, *357*, 477−479.
(12) Wang, Y. G.; Li, H. Q.; Xia, Y. Y. *Adv. Mater.* **2006**, *18*, 2619−2623.
(13) Fan, L. Z.; Hu, Y. S.; Maier, J.; Adelhelm, P.; Smarsly, B.; Antonietti, M. *Adv. Funct. Mater.* **2007**, *17*, 3083−3087.
(14) Sivakkumar, S. R.; Kim, W. J.; Choi, J. A.; MacFarlane, D. R.; Forsyth, M.; Kim, D. W. *J. Power Source* **2007**, *171*, 1062−1068.
(15) Mastragostino, M.; Arbizzani, C.; Soavi, F. *J. Power Source* **2001**, *97−98*, 812−815.
(16) Patil, D. S.; Shaikh, J. S.; Dalavi, D. S.; Karanjkar, M. M.; Devan, R. S.; Ma, Y. R.; Patil, P. S. *J. Electrochem. Soc.* **2011**, *158*, A653−A657.
(17) Nam, K. W.; Kim, K. B. *J. Electrochem. Soc.* **2006**, *153*, A81−A88.
(18) Zhou, Y.; Qin, Z. Y.; Li, L.; Zhang, Y.; Wei, Y. L.; Wang, L. F.; Zhu, M. F. *Electrochim. Acta* **2010**, *55*, 3904−3908.
(19) Jang, J.; Bae, J.; Choi, M.; Yoon, S. H. *Carbon* **2005**, *43*, 2730−2736.
(20) Huang, J.; Virji, S.; Weiller, B. H.; Kaner, R. B. *J. Am. Chem. Soc.* **2003**, *125*, 314−315.
(21) Chandrasekhar, P. *Conducting Polymers, Fundamentals and Applications: A Practical Approach*; Kluwer Academic Publishers: Boston, MA, 1999.
(22) Park, M. K.; Onishi, K.; Locklin, J.; Caruso, F.; Advincula, R. C. *Langmuir* **2003**, *19*, 8550−8554.
(23) Maity, A.; Biswas, M. *J. Ind. Eng. Chem.* **2006**, *12*, 626−634.

(24) Jang, J.; Ha, J.; Lim, B. *Chem. Commun.* **2006**, 1622−1624.
(25) Lee, S. H.; Lee, D. H.; Lee, K.; Lee, C. W. *Adv. Funct. Mater.* **2005**, *15*, 1495−1500.
(26) McNaughter, P. D.; Bear, J. C.; Steytler, D. C.; Mayes, A. G.; Nann, T. *Angew. Chem., Int. Ed.* **2011**, *50*, 10384−10387.
(27) Lees, E. E.; Nguyen, T. L.; Clayton, A. H. A.; Mulvaney, P. *ACS Nano* **2009**, *3* (5), 1121−1128.
(28) Tadokoro, H.; Seki, S.; Nitta, I. *Bull. Chem. Soc. Jpn.* **1995**, *28*, 559−564.
(29) Dmitrieva, E.; Dunsch, L. *J. Phys. Chem. B* **2011**, *115*, 6401−6411.
(30) Lee, K.; Cho, S.; Park, S. H.; Heeger, A. J.; Lee, C. W.; Lee, S. H. *Nature* **2006**, *441*, 65−68.
(31) Lee, B. H.; Park, S. H.; Back, H.; Lee, K. *Adv. Funct. Mater.* **2011**, *21*, 487−493.
(32) Lee, K. in *Encyclopedia of Nanoscience and Nanotechnology*; Nalwa, H. S., Ed.; American Scientific Publications: San Diego, CA, 2003.
(33) Tsukamoto, J. *Adv. Phys.* **1992**, *41*, 509−546.
(34) Yamaura, M.; Sato, K.; Hagiwara, T.; Iwata, K. *Synth. Met.* **1992**, *48*, 337−354.
(35) Nogami, Y.; Pouget, J. P.; Ishiguro, T. *Synth. Met.* **1994**, *62*, 257−263.
(36) Joo, J.; Oblakowski, Z.; Du, G.; Pouget, J. P.; Oh, E. J.; Wiesinger, J. M.; Min, Y.; MacDiarmid, A. G.; Epstein, A. J. *Phys. Rev. B* **1994**, *49*, 2977−2980.
(37) Pouget, J. P.; Oblakowski, Z.; Nogami, Y.; Albouy, P. A.; Laridjani, M.; Oh, E. J.; Min, Y.; MacDiarmid, A. G.; Tsukamoto, J.; Ishiguro, T.; Epstein, A. J. *Synth. Met.* **1994**, *65*, 131−140.
(38) Wang, Z. H.; Scherr, E. M.; MacDiarmid, A. G.; Epstein, A. J. *Phys. Rev. B* **1992**, *45*, 4190−4202.
(39) Menon, R.; Yoon, C. O.; Moses, D.; Heeger, A. J.; Cao, Y. *Phys. Rev. B* **1993**, *48*, 17685−17694.
(40) Menon, R.; Yoon, C. O.; Moses, D.; Heeger, A. J. In *Handbook of Conducting Polymers*, 2nd ed.; Skotheim, T. A., Elsenbaumer, R. L., Reynolds, J. R., Eds.; Dekker:, New York, 1998.
(41) Yoon, C. O.; Menon, R.; Moses, D.; Heeger, A. J. *Phys. Rev. B* **1994**, *49*, 10851−10863.
(42) Chang, Y.; Lee, K.; Kiebooms, R.; Aleshin, A.; Heeger, A. J. *Synth. Met.* **1999**, *105*, 203−206.
(43) Raghunathan, A.; Rangarajan, G.; Trivedi, D. C. *Synth. Met.* **1996**, *81*, 39−47.
(44) Lee, C.; Seo, Y. H.; Lee, S. H. *Macromolecules* **2004**, *37*, 4070−4074.
(45) Gangopadhyay, R.; De, A. *Chem. Mater.* **2000**, *12*, 608−622.
(46) Li, J.; Xie, H.; Li, Y.; Liu, J.; Li, Z. *J. Power Source* **2011**, *196*, 10775−10781.
(47) Li, Y.; Zhao, X.; Xu, Q.; Zhang, Q.; Chen, D. *Langmuir* **2011**, *27*, 6458−6463.
(48) Yan, J.; Wei, T.; Shao, B.; Fan, Z.; Qian, W.; Zhang, M.; Wei, F. *Carbon* **2010**, *48*, 487−493.
(49) Wu, Q.; Xu, Y.; Yao, Z.; Liu, A.; Shi, G. *ACS Nano* **2010**, *4*, 1963−1970.
(50) Ryu, K. S.; Kim, K. M.; Park, N. G.; Park, Y. J.; Chang, S. H. *J. Power Source* **2002**, *103*, 305−309.
(51) Li, L.; Liu, E.; Li, J.; Yang, Y.; Shen, H.; Huang, Z.; Xiang, X.; Li, W. *J. Power Source* **2010**, *195*, 1561−1521.
(52) Li, J.; Fang, J.; Cui, M.; Lu, H.; Zhang, Z. A.; Lai, Y. A. *J. Cent. South Univ. Technol* **2011**, *18*, 78−82.
(53) Xu, J.; Wang, K.; Zu, S. Z.; Han, B. H.; Wei, Z. *ACS Nano* **2010**, *4*, 5019−5026.
(54) Zhao, Y.; Bai, H.; Hu, Y.; Li, Y.; Qu, L.; Zhang, S.; Shi, G. *J. Mater, Chem.* **2011**, *21*, 13978−13983.
(55) Li, L.; Song, H.; Zhang, Q.; Yao, J.; Chen, X. *J. Power Sources* **2009**, *187*, 268−274.
(56) Liu, Q.; Nayfeh, M. H.; Yau, S. T. *J. Power Sources* **2010**, *195*, 3956−3959.
(57) Li, Y.; Zhao, X.; Xu, Q.; Zhang, Q.; Chen, D. *Langmuir* **2011**, *27*, 6458−6463.
(58) Chen, G. Y.; Cheng, Y. H.; Chou, Y. J.; Su, M. S.; Chen, C. M.; Wei, K. H. *Chem. Commun.* **2011**, *47*, 5064−5066.